Acta Geotechnica manuscript No.
(will be inserted by the editor)

Clay hypoplasticity with explicitly defined asymptotic states

David Mašín

Received: — / Accepted: —

Abstract A new rate-independent hypoplastic model for clays is developed. The model is based on the recently proposed approach enabling explicit incorporation of the pre-defined asymptotic state boundary surface and corresponding asymptotic strain rate direction into hypoplasticity. Several shortcomings of the existing hypoplastic model for clays are identified and corrected using the proposed approach. Thanks to the independent formulation of the individual model components, the new model is more suitable to form a basis for further developments and enhancements than the original one.

Keywords hypoplasticity · asymptotic behaviour · clay · state boundary surface

1 Introduction

Hypoplasticity, a constitutive theory especially suitable for modelling the behaviour of frictional materials, has originally been developed to predict the behaviour of granular materials such as sand or gravel [21, 53, 8, 51, 5]. Since the last decade, its modifications for fine grained soils have been developed by several researchers. In particular, Niemunis [39] developed a rate-dependent viscohypoplastic model for clays as a combination of hypoplasticity with Modified Cam-clay [46] yield condition. Niemunis et al. [40] further enhanced this model by the effects of stregth anisotropy and irreversibility of the response within the state boundary surface. Gudehus [9] enhanced his earlier model from [8] by viscous effects. The other hypoplastic models do not consider viscosity. Herle and Kolymbas [16] modified the model by von Wolffersdorff [51] to predict the rate-independent behaviour of soils with low friction angles. This model was later improved by Mašín [24] by reducing number of parameters and considering asymptotic states which better represent the fine-grained soil behaviour. Further, Weifner and Kolymbas [49] developed a hypoplastic model aimed to simulate the behaviour of both sand and clay. Youwai et al. [54] modified this model to simulate the behaviour of Bangkok soft clay. Huang et al. [18] developed a model suitable for predicting the behaviour of normally consolidated clays.

In this work, we focus on further development of the model by Mašín [24]. This model has been developed in 2005 and since then it has been thoroughly evaluated, it was applied in simulation of boundary value problems and served as a basic model for further enhancements. The evaluation of the model can be found in Mašín et al. [36] and Hájek et al. [13], who compared its predictive capabilities with other elasto-plastic and hypoplastic models. Weifner and Kolymbas [50] compared its predictions with the earlier hypoplastic model for soils with low friction angles by Herle and Kolymbas [16]. Gudehus and Mašín [12] demonstrated the model performance using suitably chosen graphical representation. Mašín and Herle [32] investigated certain consequences of the model mathematical formulation (existence and shape of the asymptotic state boundary surface), and Mašín and Herle [33] proposed a modification of the model that corrects the shape of the undrained stress path of normally consolidated soils, inspired by the work from Huang et al. [18].

David Mašín
Charles University in Prague, Faculty of Science, Albertov 6, 12843 Prague 2, Czech Republic
Tel.: +420-2-21951552
Fax: +420-2-21951556
E-mail: masin@natur.cuni.cz

The model implementation for different finite element codes is freely available on the internet (Gudehus et al. [11]) and the model has been used in simulations of boundary value problems. Mašín [26], Svoboda et al. [48] and Svoboda and Mašín [47] applied it in simulation of tunnelling problems in stiff clays, Mašín et al. [31] simulated deep excavation in soft clay deposit, Ali et al. [1] used the model to simulate undrained cavity expansion. Herle et al. [17] adopted the model in a complex probabilistic evaluation of properties of soils from coal mining deposits. Miča et al. [37] used the model in simulations of deep excavations in stiff clays.

The model has also been used as a driver for including different special effects. Mašín [25] included the effects of meta-stable structure (further evaluation of that model may be found in Reference [27]). Mašín and Khalili [34] developed a model for unsaturated soil. This model, combined with the water retention model by Mašín [28], has been compared with different constitutive models for unsaturated soils in a benchmark test described by D'Onza et al. [6]. The evaluation have demonstrated good performance of unsaturated hypoplastic model, coming along with relatively low number of material parameters. Furthermore, Najser et al. [38] included the effects of lumpy structure, and Mašín and Khalili [35] included both the effects of partial saturation and temperature on soil behaviour.

Hypoplasticity in its basic form, including the model developed in this paper, cannot predict the soil behaviour in the small to very small strain range, and consequently it is also unsuitable for predicting the cyclic soil response. To overcome this shortcoming, the model must be extended. One of the approaches is the concept of intergranular strains (Niemunis and Herle [41]); recently, another ways of the model enhancement have been proposed, such as the incorporation of the loading surface concept [7]. Even an enhanced model, however, is not ideal for predicting the cyclic response at very high number of cycles. In such cases, different approaches may be used, such as those proposed by Niemunis et al. [43, 42, 44].

2 Limitations of the original clay hypoplastic model

Since its development, the hypoplastic model from Ref. [24] has been thoroughly evaluated and several shortcomings have been identified.

In particular, Mašín and Herle [32] studied the shape of the asymptotic state boundary surface (ASBS) predicted by this model. The asymptotic state boundary surface represents all asymptotic states in the stress vs. void ratio space. The asymptotic states are those achieved asymptotically after sufficiently long stretching with constant strain rate direction. For more information on asymptotic soil behaviour, see [29].

Mašín and Herle [32] observed that the shape of ASBS can be extracted from the hypoplastic model formulation, and that it depends on the combination of material parameters. For high ratios κ^*/λ^*, the model predicts unrealistic shape of the ASBS, as shown in Fig. 1. This dependency of ASBS on material parameters is not underlined by any physical phenomena, and is simply an undesired consequence of the particular model formulation.

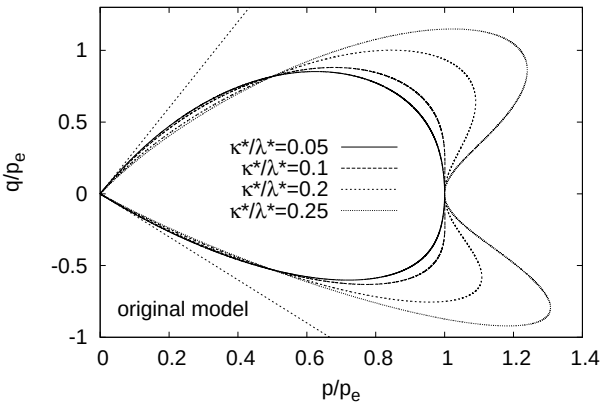

Fig. 1 The shape of the ASBS predicted by the original hypoplastic model, with different values of the parameter κ^* (the remaining parameters given in Tab. 1, label "eval.").

The second limitation of the model is related to difficulties in its further enhancements. Mašín and Herle [32] have shown that the shape of the ASBS of the model depends on the constitutive tensor $\boldsymbol{\mathcal{L}}$. The model can be enhanced by the so-called intergranular strain concept (Niemunis and Herle [41]), which allows to predict high very small strain stiffness and the stiffness dependency on recent history of deformation. The very small strain stiffness is governed by the tensor $\boldsymbol{\mathcal{L}}$. The tensor $\boldsymbol{\mathcal{L}}$ of the original model has several undesired properties – for example, it does not allow to specify inherent stiffness anisotropy, often observed on samples of undisturbed clay. Any modification of the tensor $\boldsymbol{\mathcal{L}}$ of the original model, however, improperly changes also the shape of the ASBS, and the possibility of further development of the model is thus limited.

In some cases, the original model was found to predict improperly the development of stiffness with shear strain. As an example, Figure 2 shows shear strain – deviatoric stress curve of an undrained shear test on Dortmund clay from [17] (more details in Sec. 8.2). The model predicts a sharp bend of the stress – strain curve

at the shear strain level of approximately 5%, whereas the experiment shows more gradual stiffness decrease. This inaccuracy cannot be eliminated by modification of the material parameters.

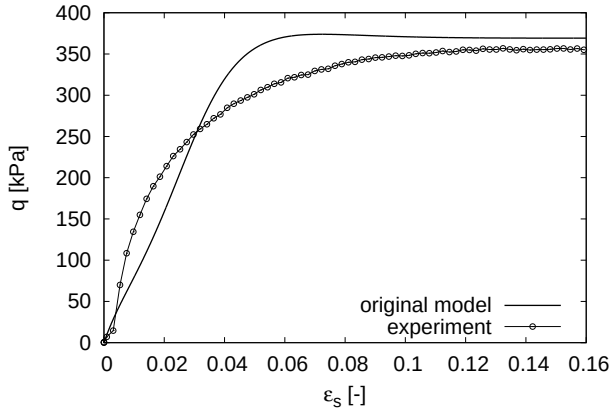

Fig. 2 Shear strain vs. deviator stress curve of a triaxial undrained shear test on Dortmund clay, together with simulation by the original clay hypoplastic model.

3 Explicit incorporation of asymptotic states into hypoplasticity

A procedure for explicit incorporation of the asymptotic states into hypoplasticity has been proposed by Mašín [30], and we will adopt this approach herein. A general formulation of the hypoplastic model may be written as [8]

$$\mathring{\mathbf{T}} = f_s \left(\boldsymbol{\mathcal{L}} : \mathbf{D} + f_d \mathbf{N} \|\mathbf{D}\| \right) \tag{1}$$

where $\mathring{\mathbf{T}}$ and $\mathbf{D}$ represent the objective (Zaremba-Jaumann) stress rate and the Euler stretching tensor respectively, $\boldsymbol{\mathcal{L}}$ and $\mathbf{N}$ are fourth- and second-order constitutive tensors, f_s is the factor controlling the influence of mean stress (barotropy factor) and f_d is the factor controlling the influence of relative density (pyknotropy factor).

To evaluate the model response at the ASBS, we will interpret it in the stress space normalised by the size of the constant void ratio cross-section through the ASBS. It is given by the Hvorslev equivalent pressure p_e, defined as a mean stress at the isotropic normal compression line at the current void ratio e. The normalised stress thus reads $\mathbf{T}_n = \mathbf{T}/p_e$ and it follows that

$$\dot{\mathbf{T}}_n = \frac{\partial}{\partial t}\left(\frac{\mathbf{T}}{p_e}\right) = \frac{\dot{\mathbf{T}}}{p_e} - \frac{\mathbf{T}}{p_e^2}\dot{p}_e \tag{2}$$

The objective (Zaremba-Jaumann, see, e.g., [22]) rate of the normalised stress $\mathring{\mathbf{T}}_n$, which vanishes for pure rigid body rotation, is given by

$$\mathring{\mathbf{T}}_n = \dot{\mathbf{T}}_n + \mathbf{T}_n \cdot \mathbf{W} - \mathbf{W} \cdot \mathbf{T}_n \tag{3}$$

where the spin tensor $\mathbf{W}$ is the skew-symmetric part of the velocity gradient. Combination of (2) and (3) yields

$$\mathring{\mathbf{T}}_n = \frac{1}{p_e}\left(\dot{\mathbf{T}} + \mathbf{T}\cdot\mathbf{W} - \mathbf{W}\cdot\mathbf{T} - \frac{\mathbf{T}}{p_e}\dot{p}_e\right) = \frac{\mathring{\mathbf{T}}}{p_e} - \frac{\mathbf{T}}{p_e^2}\dot{p}_e \tag{4}$$

In the following, we assume normal compression lines linear in the $\ln(1+e)$ vs. $\ln p/p_r$ plane [3] (p_r is the reference stress of 1 kPa). The isotropic normal compression line can be written as

$$\ln(1+e) = N - \lambda^* \ln(p_e/p_r) \tag{5}$$

where N and λ^* are model parameters. It follows that

$$p_e = p_r \exp\left[\frac{N - \ln(1+e)}{\lambda^*}\right] \tag{6}$$

and thus

$$\dot{p}_e = -\frac{p_e}{\lambda^*}\left(\frac{\dot{e}}{1+e}\right) = -\frac{p_e}{\lambda^*}\operatorname{tr}\mathbf{D} \tag{7}$$

Combination of (7), (4) and (1) implies that

$$\mathring{\mathbf{T}}_n = \frac{f_s}{p_e}\left(\boldsymbol{\mathcal{L}} : \mathbf{D} + f_d \mathbf{N}\|\mathbf{D}\|\right) + \frac{\mathbf{T}}{p_e \lambda^*}\operatorname{tr}\mathbf{D} \tag{8}$$

During asymptotic stretching the stress state remains fixed in the $\mathbf{T}_n$ space [32], provided the constant void ratio cross-sections through the ASBS differ only in size and not in shape. This condition implies $\mathring{\mathbf{T}}_n = \mathbf{0}$. It then follows from (8) that

$$-\frac{\mathbf{T}}{\lambda^*}\operatorname{tr}\mathbf{D}^A = f_s\left(\boldsymbol{\mathcal{L}} : \mathbf{D}^A + f_d^A \mathbf{N}\|\mathbf{D}^A\|\right) \tag{9}$$

where f_d^A is the value of f_d at the ASBS and $\mathbf{D}^A$ is the asymptotic strain rate corresponding to the given stress state. Eq. (9) can be manipulated in the following way:

$$-\left(\frac{\mathbf{T}}{\lambda^*}\operatorname{tr}\mathbf{D}^A + f_s \boldsymbol{\mathcal{L}} : \mathbf{D}^A\right) = f_s f_d^A \mathbf{N}\|\mathbf{D}^A\| \tag{10}$$

$$-\boldsymbol{\mathcal{A}} : \mathbf{D}^A = f_s f_d^A \mathbf{N}\|\mathbf{D}^A\| \tag{11}$$

$$-\boldsymbol{\mathcal{A}} : \boldsymbol{d} = f_s f_d^A \mathbf{N} \tag{12}$$

where

$$\boldsymbol{\mathcal{A}} = f_s \boldsymbol{\mathcal{L}} + \frac{\mathbf{T}}{\lambda^*} \otimes \mathbf{1} \tag{13}$$

$$\boldsymbol{d} = \frac{\mathbf{D}^A}{\|\mathbf{D}^A\|} \tag{14}$$

Eq. (12) implies that

$$\mathbf{N} = -\frac{\boldsymbol{\mathcal{A}} : \boldsymbol{d}}{f_s f_d^A} \tag{15}$$

Combining (15) with (1) yields an alternative expression of the hypoplastic model

$$\mathring{\mathbf{T}} = f_s \boldsymbol{\mathcal{L}} : \mathbf{D} - \frac{f_d}{f_d^A} \boldsymbol{\mathcal{A}} : \boldsymbol{d} \|\mathbf{D}\| \tag{16}$$

An arbitrary shape of the ASBS can be incorporated into hypoplasticity with the aid of Eq. (16), by appropriate specification of the dependence of f_d^A on the void ratio and stress ratio. The corresponding asymptotic direction of the strain rate is then prescribed by $\boldsymbol{d}$. This can be done independently of the selected expression for the tensor $\boldsymbol{\mathcal{L}}$. Formulation of the ASBS shape and asymptotic strain rate direction $\boldsymbol{d}$ proposed for the new model is detailed in the following two sections.

4 Proposed shape of the asymptotic state boundary surface

The shape of the asymptotic state boundary surface should have certain properties to ensure good representation of the experimental data and a physical consistency. The following requirements have been considered:

1. Deviatoric (constant mean stress) cross-sections through the ASBS should correspond to the failure criterion by Matsuoka and Nakai [23].
2. Mobilised friction angle φ_m should be equal to the critical state friction angle φ_c at $p_e/p = 2$. This specifies the position of the critical state line in the $\ln p$ vs. $\ln(1+e)$ plane.
3. φ_m for $p_e/p = 1$ should be equal to zero to predict the isotropic asymptotic state.
4. φ_m for $p_e/p \to \infty$ should limit to $\varphi_m \to 90°$. This ensures that the ASBS does not span into the tensile stress region.

The following expression is proposed which satisfies these properties:

$$f = 0 = F_m + \left(\frac{p}{p_e}\right)^{\omega} - 1 \tag{17}$$

where F_m is the Matsuoka-Nakai factor, which may be seen as an equivalent to the mobilised friction angle φ_m (with $F_m = \sin^2 \varphi_m$) corresponding to the Matuoka-Nakai failure criterion[1]. It is calculated as [23]

$$F_m = \frac{9 I_3 + I_1 I_2}{I_3 + I_1 I_2} \tag{18}$$

[1] Note that the requirement No. 4 is satisfied only approximately with the condition by Matsuoka and Nakai [23], as $F_m = 1$ does not exactly represent the boundary of compressive stresses.

with stress invariants I_1, I_2 and I_3:

$$I_1 = \mathrm{tr}\mathbf{T} \tag{19}$$

$$I_2 = \frac{1}{2}\left[\mathbf{T} : \mathbf{T} - (I_1)^2\right] \tag{20}$$

$$I_3 = \det\mathbf{T} \tag{21}$$

Eq. (17) can also be expressed as

$$\left(\frac{p}{p_e}\right)^{\omega} = 1 - \sin^2 \varphi_m \tag{22}$$

which is an equation of parabola of the form $y = 1 - x^2$, where $x = \sin\varphi_m$ and $y = \left(\frac{p}{p_e}\right)^{\omega}$. For $p/p_e = 1$ the model predicts $\varphi_m = 0$ (isotropic stress state). For $p_e/p \to \infty$ the mobilised friction angle limits to $\varphi_m \to 90°$. The exponent ω is expressed to ensure that for $p_e/p = 2$ mobilised friction angle equals to φ_c. To derive a suitable expression for ω, $p_e/p = 2$ and $\varphi_m = \varphi_c$ is substituted into Eq. (22):

$$\left(\frac{1}{2}\right)^{\omega} = 1 - \sin^2 \varphi_c \tag{23}$$

which yields

$$\omega = -\frac{\ln\left(\cos^2 \varphi_c\right)}{\ln 2} \tag{24}$$

Additional freedom in the calibration of the shape of ASBS is gained by the following modification of (24):

$$\omega = -\frac{\ln\left(\cos^2 \varphi_c\right)}{\ln 2} + a\left(F_m - \sin^2 \varphi_c\right) \tag{25}$$

The additional term does not influence predictions at the isotropic, critical and $p_e/p \to \infty$ states, but controls the shape of ASBS at the other states through the shape factor a, as shown in Fig. 3. If needed, a can be considered as a material parameter controlling peak friction angle of overconsolidated soil (Fig. 3). In the present simulations, however, a fixed value of $a = 0.3$ has been used. This yields the state boundary surface close to the elliptic shape of the ASBS of the Modified Cam clay model [46] in the range $p > p_e/2$.

The shape of the ASBS, calculated using Eqs. (17-25), is in Fig. 4a plotted for the axisymmetric stress state in the normalised stress plane p/p_e vs. q/p_e for different critical state friction angles. The ASBS has the desired properties summarised above. Fig. 4b shows the shape of the ASBS of the original hypoplastic model, calculated using procedure from [32]. The ASBS of the original model has also the required properties; its shape, however, depends on the other material parameters. For comparison, Fig. 4c shows the ASBS of the Modified Cam-clay model. The proposed model predicts similar shape of the ASBS in compression for $p_e/p < 2$.

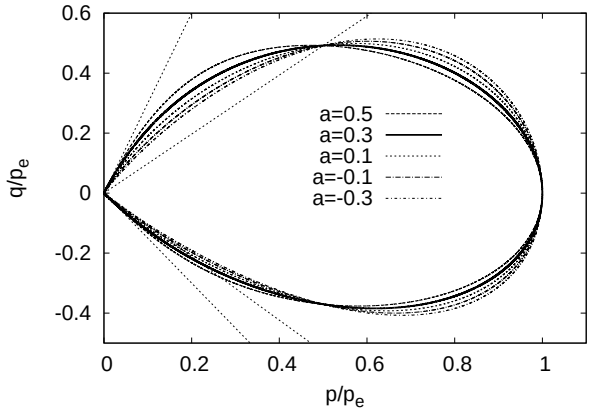

Fig. 3 The influence of a from Eq. (25) on the shape of the ASBS of the proposed model. $a = 0.3$ selected as a standard value.

Otherwise, the Modified Cam-clay model predicts non-realistic shape of the ASBS. In particular, it spans into the tensile stress region and overpredicts critical state friction angle in extension.

Figure 5 shows various 3D-views of the ASBS of the proposed model in the principal stress space for $\varphi_c = 25°$. In particular, Figure 5 demonstrates that the ASBS inherits properties of the Matsuoka-Nakai failure criterion, which has circular deviatoric cross-sections for $\varphi_m \to 0°$ (Fig. 5d) and triangular cross-sections for $\varphi_m \to 90°$ (Fig. 5e).

5 Proposed asymptotic strain rate direction

The basic properties of the asymptotic strain rate direction, expressed here as $\boldsymbol{d} = \boldsymbol{d}^A/\|\boldsymbol{d}^A\|$, have been discussed in References [12,10,29]. Therein, $\boldsymbol{d}^A$ is represented in terms of the dependency of the angles ψ_σ and $\psi_{\dot\epsilon}$ (Fig. 6). This dependency should have the following properties:

1. For prediction of the isotropic state, zero shear strains ($\operatorname{dev} \boldsymbol{d}^A = \boldsymbol{0}$) should be predicted for $\varphi_m = 0°$.
2. For prediction of the critical state, zero volumetric strains ($\operatorname{tr} \boldsymbol{d}^A = 0$) should be predicted for $\varphi_m = \varphi_c$.
3. For prediction of the K_0 state, K_0 should agree with the empirical formula by Jáky [19]

$$K_0 = 1 - \sin\varphi_c \tag{26}$$

4. The limitting directions $\pm d$ should correspond to the mobilised friction angles of 90°. As noted by Gudehus [10] (Chapters 2 and 3), these dilatant state limits correspond to the onset of cracking. Although they are somewhat fictitious, they represent reasonable limit bounds.

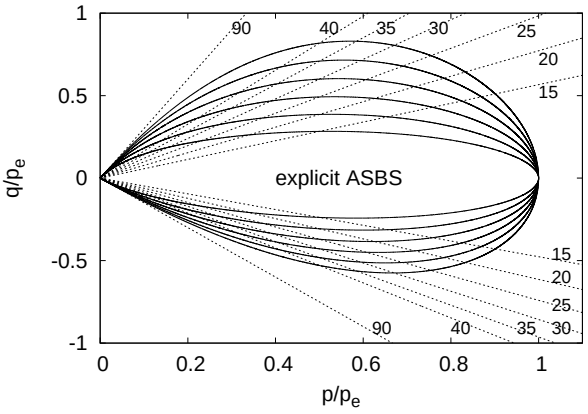

(a)

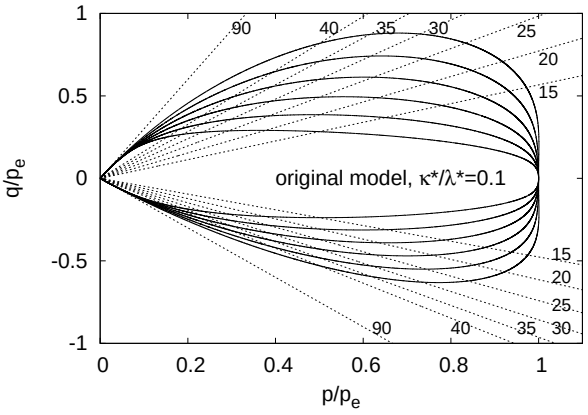

(b)

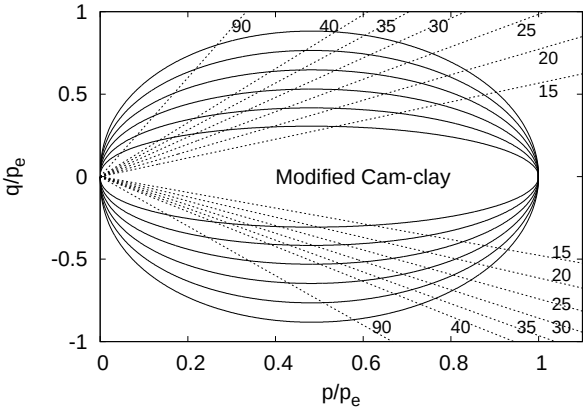

(c)

Fig. 4 Asymptotic state boundary surfaces for critical state friction angles $\varphi_c = 15°, 20°, 25°, 30°, 35°, 40°$. Dashed lines represent constant mobilised friction angle lines (labels in degrees). (a) proposed model, (b) original model for $\kappa^*/\lambda^* = 0.1$, (c) Modified Cam-clay model.

5. $\boldsymbol{d}^A$ should have a radial deviatoric direction. This is supported by experimental studies from References [52,2,20,4].

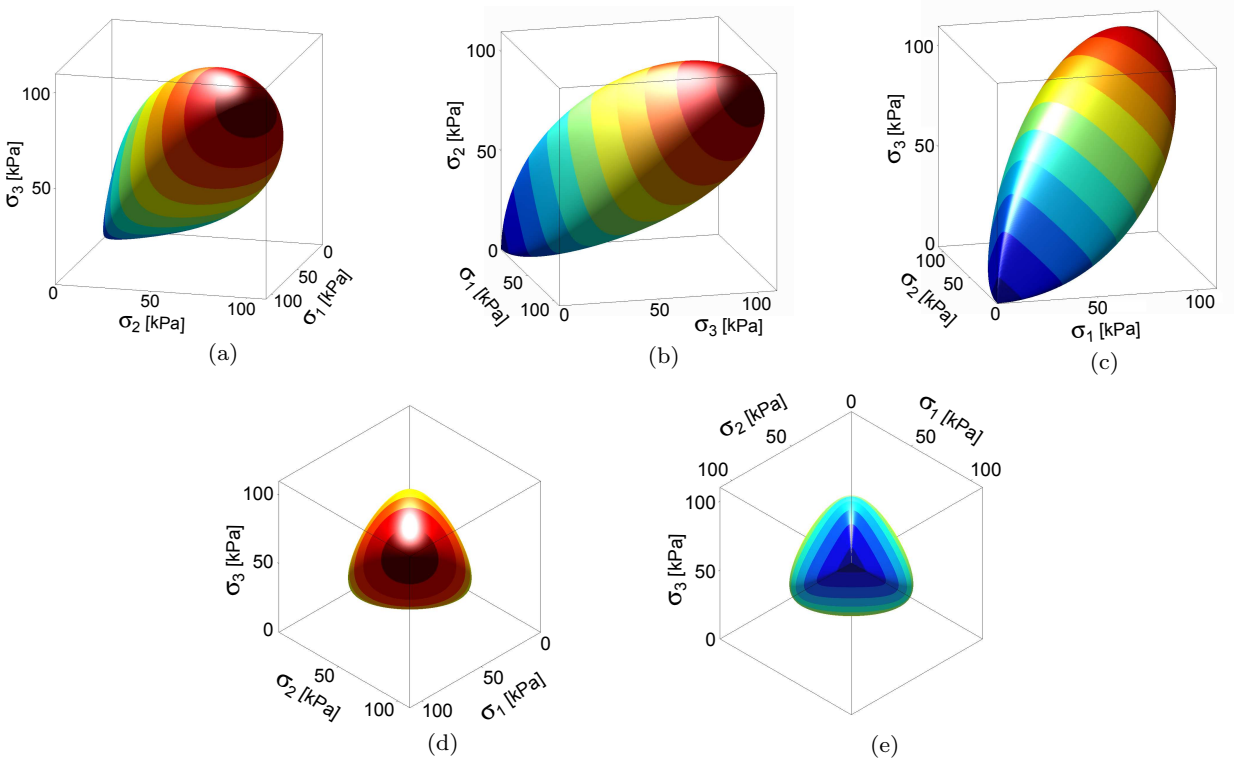

Fig. 5 Principal stress space 3D plots of the ASBS of the proposed model for $\varphi_c = 25°$. (a,b,c) views from various angles; (d) deviatoric view for $\varphi_m \leq \varphi_c$; (e) deviatoric view for $\varphi_m \geq \varphi_c$. Color transitions represent constant mean stress cuts.

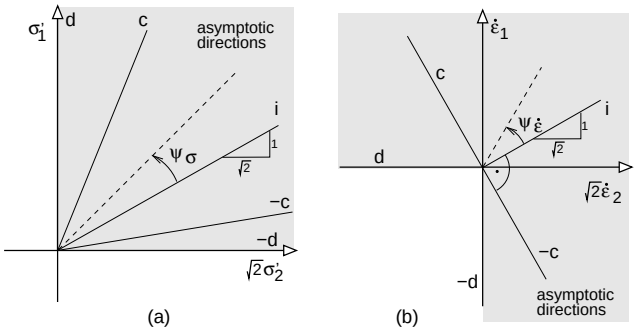

Fig. 6 Definition of angles ψ_σ and $\psi_{\dot\epsilon}$ used in representation of the asymptotic strain rate direction (from [12,10,29]).

The expression for $\boldsymbol{d}^A$ will be set in the form

$$\boldsymbol{d}^A = -\hat{\mathbf{T}}^* + \mathbf{1}X \tag{27}$$

with $\hat{\mathbf{T}}^*$, which is defined as $\hat{\mathbf{T}}^* = \hat{\mathbf{T}} - \mathbf{1}/3$, where $\hat{\mathbf{T}} = \mathbf{T}/\operatorname{tr}\mathbf{T}$. Eq. (27) directly satisfies properties 1 and 5 for any positive X. Next, the dependency of X on mobilised friction angle is introduced. With $X = 0$ for $\varphi_m = \varphi_c$, property 2 is ensured. To include property 4, $X = 2/3$ for $\varphi_m = 90°$ in triaxial compression and $X = 1/6$ for $\varphi_m = 90°$ in triaxial extension.

The following expression for X satisfying these properties is proposed

$$X = \left[\frac{2}{3} - \frac{\cos 3\theta + 1}{4} F_m^{1/4}\right] \frac{F_m^{\xi/2} - \sin^\xi \varphi_c}{1 - \sin^\xi \varphi_c} \tag{28}$$

where the Lode angle θ is defined as

$$\cos 3\theta = -\sqrt{6}\frac{\operatorname{tr}\left(\hat{\mathbf{T}}^* \cdot \hat{\mathbf{T}}^* \cdot \hat{\mathbf{T}}^*\right)}{\left[\hat{\mathbf{T}}^* : \hat{\mathbf{T}}^*\right]^{3/2}} \tag{29}$$

$\cos 3\theta = -1$ in triaxial compression and $\cos 3\theta = 1$ in triaxial extension. The factor ξ controls the ratio of volumetric and shear strains for φ_m other than 0°, φ_c and 90°. ξ was found by an optimisation procedure to make sure the strain rate direction satisfies approximately the Jáky [19] formula:

$$\xi = 1.7 + 3.9 \sin^2 \varphi_c \tag{30}$$

Finally, the expression for $\boldsymbol{d}^A$ is as follows:

$$\boldsymbol{d}^A = -\hat{\mathbf{T}}^* + \mathbf{1}\left[\frac{2}{3} - \frac{\cos 3\theta + 1}{4} F_m^{1/4}\right] \frac{F_m^{\xi/2} - \sin^\xi \varphi_c}{1 - \sin^\xi \varphi_c} \tag{31}$$

The proposed formulation and the original model yield similar ψ_σ and $\psi_{\dot\epsilon}$ dependencies, coinciding at

isotropic (i) and critical ($\pm c$) states. Unlike the original model, however, the proposed formulation properly considers also the limitting direction $\pm d$.

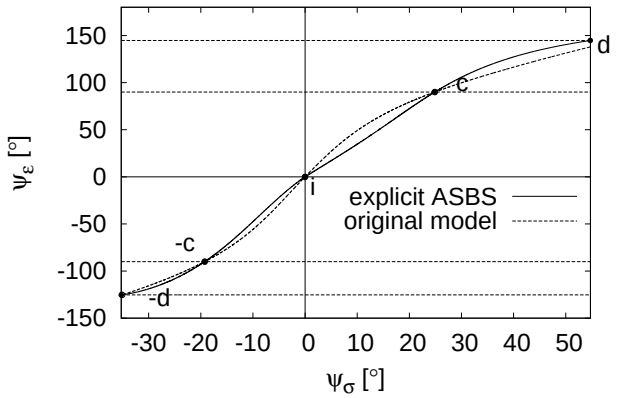

Fig. 7 Asymptotic strain rate direction demonstrated in terms of angles ψ_σ and $\psi_{\dot\varepsilon}$ for the proposed and original models.

Figure 8 shows K_0 values predicted by the proposed, original and Modified Cam-clay models for different values of φ_c ($\kappa^*/\lambda^* = 0.1$ for the original model). The proposed model predicts K_0 practically coinciding with the Jáky [19] equation (26). Both the original and Cam-clay models overpredict K_0.

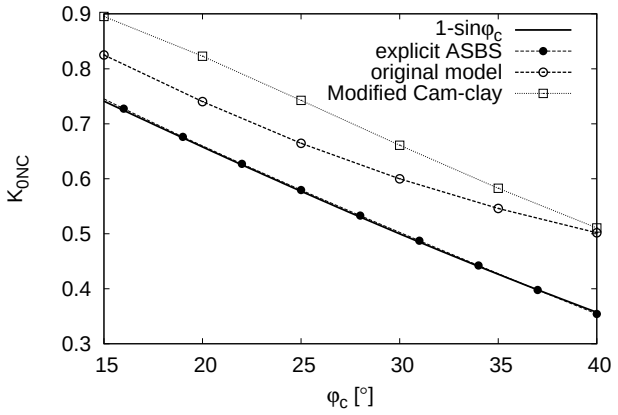

Fig. 8 K_0 values for different φ_c predicted by the proposed, original and Modified Cam-clay models ($\kappa^*/\lambda^* = 0.1$ for the original model).

6 Model formulation

In this section, complete formulation of the new hypoplastic model is described, adopting a general approach from Sec. 3, with ASBS shape from Sec. 4 and asymptotic strain rate direction from Sec. 5.

General rate formulation of the model is given by Eq. (16). The tensor $\boldsymbol{\mathcal{L}}$ is represented by isotropic elasticity: that is

$$\boldsymbol{\mathcal{L}} = \boldsymbol{\mathcal{I}} + \frac{\nu}{1-2\nu}\mathbf{1}\otimes\mathbf{1} \tag{32}$$

where the parameter ν controls the proportion of bulk and shear stiffness. Effectively, it regulates the shear stiffness, since the bulk stiffness in the model is controlled by the parameters λ^* and κ^* (as shown later).

The asymptotic strain rate direction $\boldsymbol{d}$ is specified by

$$\boldsymbol{d} = \frac{\boldsymbol{d}^A}{\|\boldsymbol{d}^A\|} \tag{33}$$

where $\boldsymbol{d}^A$ is given by Eq. (31).

The following expression for the factor f_d, which governs the non-linear behaviour inside the state boundary surface, is chosen:

$$f_d = \left(\frac{2p}{p_e}\right)^\alpha \tag{34}$$

where $\alpha = 2$ is controlling the influence of OCR on non-linear response inside the ASBS. The value of f_d^A, needed in Eq. (16), is calculated using Eq. (34) combined with the proposed ASBS formulation (Sec. 4). Eq. (17) gives

$$p^A = p_e\,(1-F_m)^{1/\omega} = p_e\left(\frac{-8I_3}{I_3 + I_1 I_2}\right)^{1/\omega} \tag{35}$$

where p^A is the mean stress at the ASBS for the given φ_m. Combination of (35) with (34) yields the expression for f_d^A:

$$f_d^A = 2^\alpha (1-F_m)^{\alpha/\omega} \tag{36}$$

The last component of the model to be defined is the factor f_s. It is specified to ensure that the slope of the isotropic unloading line in the $\ln(1+e)$–$\ln p$ plane, for unloading starting from the isotropic normally consolidated state, is given by κ^*. Note that the slope λ^* of the isotropic normal compression line is already implicit in the model formulation, since it has been adopted as a primary assumption in the derivation of the tensor $\boldsymbol{\mathcal{A}}$. Algebraic manipulations with the above tensorial equations reveal that for unloading (volume increase, $\dot e > 0$), the isotropic form of the model is given as:

$$\dot p = \left[\frac{p}{\lambda^*} - 2f_s\left(\frac{1}{3} + \frac{\nu}{1-2\nu}\right)\right]\frac{\dot e}{1+e} \tag{37}$$

Eq. (37) can be compared with $\dot{e}/(1+e) = -\kappa^* \dot{p}/p$, which leads to an expression for f_s

$$f_s = \frac{3p}{2}\left(\frac{1}{\lambda^*} + \frac{1}{\kappa^*}\right)\frac{1-2\nu}{1+\nu} \tag{38}$$

A complete formulation of the proposed hypoplastic model is summarised in Appendix.

7 Model parameters

The model requires five parameters, with the same physical interpretation as the parameters of the Modified Cam-clay model: φ_c, λ^*, κ^*, N and ν. φ_c is the critical state friction angle; λ^* is the slope of the isotropic normal compression line in the plane $\ln(1+e)$ vs. $\ln p$; κ^* controls slope of unloading line in the same plane; N is the value of $\ln(1+e)$ at the isotropic normal compression line for $p = p_r = 1$ kPa; and finally the parameter ν controls the shear stiffness.

The parameter ν has the same effect as the parameter r of the original clay hypoplastic model. In fact, a direct relation between ν of the proposed model and r of the original model may be found, which reads

$$\nu = \frac{3r\,(\lambda^* + \kappa^*) - 4\kappa^*}{6r\,(\lambda^* + \kappa^*) + 4\kappa^*} \tag{39}$$

The proposed hypoplastic model can thus be used in place of the original one without a need for additional calibration.

The proposed model can be applied in combination with the intergranular strain concept by Niemunis and Herle [41] in order to predict properly the soil behaviour in the very small strain range. While using this concept, the very small strain stiffness matrix $\boldsymbol{\mathcal{M}}$ is given by

$$\boldsymbol{\mathcal{M}} = m_R f_s \boldsymbol{\mathcal{L}} \tag{40}$$

where m_R is a model parameter controlling the shear modulus. The adopted formulation of the tensor $\boldsymbol{\mathcal{L}}$ implies that

$$\boldsymbol{\mathcal{M}} = 2G_0 \boldsymbol{\mathcal{L}} \tag{41}$$

where G_0 is the very small strain shear modulus. Comparison of (41) and (40) with the aid of the adopted formulation for the factor f_s (Eq. (38)) enables us to calculate the value of the parameter m_R from the known very small strain shear modulus G_0 as

$$m_R = \frac{4G_0}{3p}\left(\frac{1+\nu}{1-2\nu}\right)\left(\frac{\lambda^*\kappa^*}{\lambda^* + \kappa^*}\right) \tag{42}$$

With this parameter m_R and the relation between ν and r from Eq. (39), the proposed and original models predict identical very small strain shear moduli.

8 Model predictions

8.1 Qualitative comparison with the original model

First, the proposed model will be compared with the original one using different means of graphical representation. Parameters used in this evaluation are given in Tab. 1, label "eval." (note these parameters do not correspond to any particular soil experimental data set). Figure 9 shows the shape of the ASBS, together with response envelopes for different states of stress and overconsolidation. For details on response envelope representation, see Gudehus and Mašín [12]. Because the used parameter set involves parameters which imply reasonable shape of the ASBS of the original model, the two graphs are very similar. In fact, there is only one substantial difference in the response of the two models; the original model produces response envelopes which rotate with increasing stress deviator, whereas the proposed model adopts isotropic elasticity, which means that the shape of the response envelopes is not affected by the stress state. The different formulation of the tensor $\boldsymbol{\mathcal{L}}$ influences the model predictions inside the ASBS, and in most cases causes the proposed model to better reproduce the experimental data. This will be shown later in Sec. 8.2.

soil	φ_c	λ^*	κ^*	N	ν/r
eval.	25°	0.1	0.01	1	0.2/0.242
Kaolin	27.5°	0.065	0.01	0.918	0.35/0.67
Dortmund	27.9°	0.057	0.008	0.749	0.38/0.94
Weald (prop.)	24°	0.059	0.014	0.8	0.3 (ν)
(orig.)			0.018		0.65 (r)
Brno	22°	0.128	0.015	1.51	0.33/0.45
Koper	33°	0.103	0.015	1.31	0.28/0.3

Table 1 Parameters of the proposed and original models used in the simulations (ν specified for the proposed model, r for the original). "eval." denote fictitious parameters used in evaluation of the model response in Sec. 8.1.

Figure 10 demonstrates an approach to asymptotic states from some arbitrary state within the asymptotic state boundary surface. This figure shows stress paths of constant $\psi_{\dot{\epsilon}}$ tests plotted in the normalised q/p_e^* vs. p/p_e^* plane, together with so-called normalised incremental response envelopes (NIREs, see Mašín et al. [36] for more details) for different strain levels. In both models, the stress paths and NIREs ultimately converge to the ASBS. The proposed model predicts more straight approach to asymptotic states and slightly different shapes of NIREs. This is, again, predominantly caused by the different formulation of the $\boldsymbol{\mathcal{L}}$ tensor.

Figure 11 shows normalised undrained stress paths and normalised deviatoric stress - shear strain curves

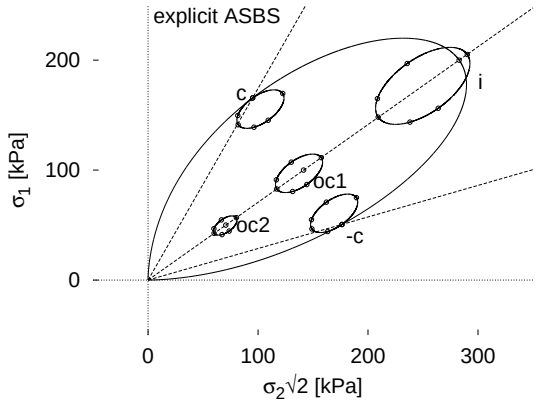

(a)

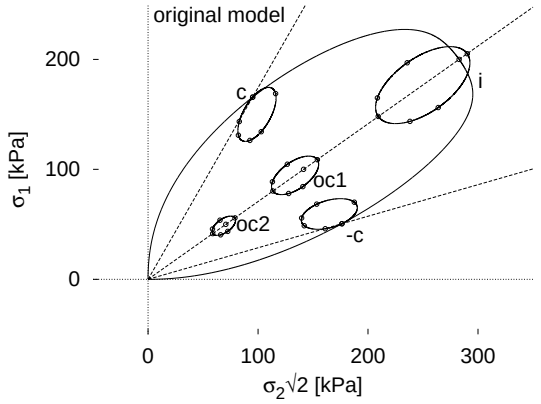

(b)

Fig. 9 The shape of ASBS of the original and proposed models, plotted together with response envelopes at the isotropic (i) and critical ($\pm c$) asymptotic states and in two overconsolidated (oc) states.

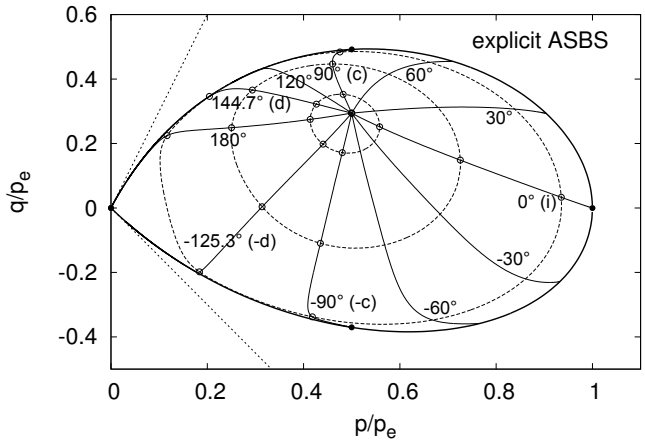

(a)

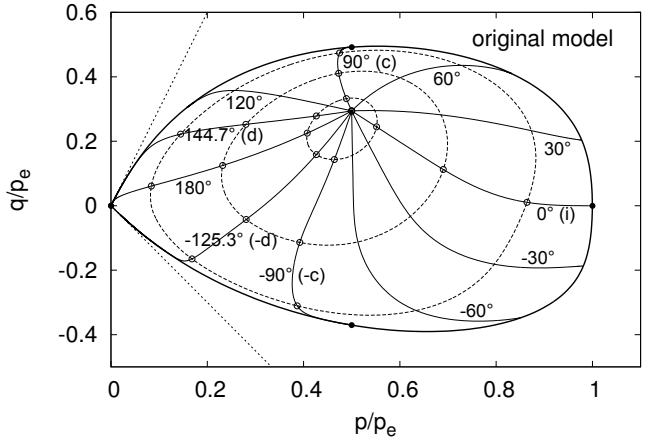

(b)

Fig. 10 Stress paths of constant $\psi_{\dot{\epsilon}}$ tests and incremental response envelopes plotted in the normalised q/p_e^* vs. p/p_e^* space for tests starting from a common arbitrary state within ASBS. Values of angles $\psi_{\dot{\epsilon}}$ in constant $\psi_{\dot{\epsilon}}$ tests specified in labels, incremental response envelopes plotted for $\|\boldsymbol{\epsilon}\| = 0.002, 0.008, 0.02, 0.5$ (the $\|\boldsymbol{\epsilon}\| = 0.5$ NIRE coincides with the ASBS).

of the original (b,d) and proposed (a,c) models. The initial states are located along K_0 unloading line. First of all, it is clear that the models predict different K_0 values (q/p values at K_0). Similarly to the observation from Fig. 9, the proposed model predicts more straight approach to the asymptotic state. Unlike the original model, the proposed model predicts stress path of the undrained compression test on normally consolidated specimen which approximately follows the ASBS. This better reproduces the soil behaviour, as discussed by Mašín and Herle [33]. The two models also predict slightly different rates of stiffness decrease. This issue will be discussed in more detail in Sec. 8.2.

8.2 Evaluation using experimental data

In this section, predictions of proposed and original models will be compared with the experimental data on different fine-grained soils. The evaluation of the original model using these data have already been presented in previous publications, where an interested reader can find additional details. Parameters used in the simulations are summarised in Table 1. Note that ν was not always calculated from r using Eq. (39), but it was calibrated specifically to obtain the best match with the experimental data.

Reconstituted kaolin: The experiments on reconstituted kaolin clay have been performed by Hattab and Hicher [14] and adopted for evaluation of different constitutive models by Hájek et al. [13]. The specimens of kaolin clay with Atterberg limits w_L 40% and w_P 20% were prepared in a consolidometer from a slurry at a water content of twice the liquid limit. The specimens were isotropically loaded up to the maximum preconsolida-

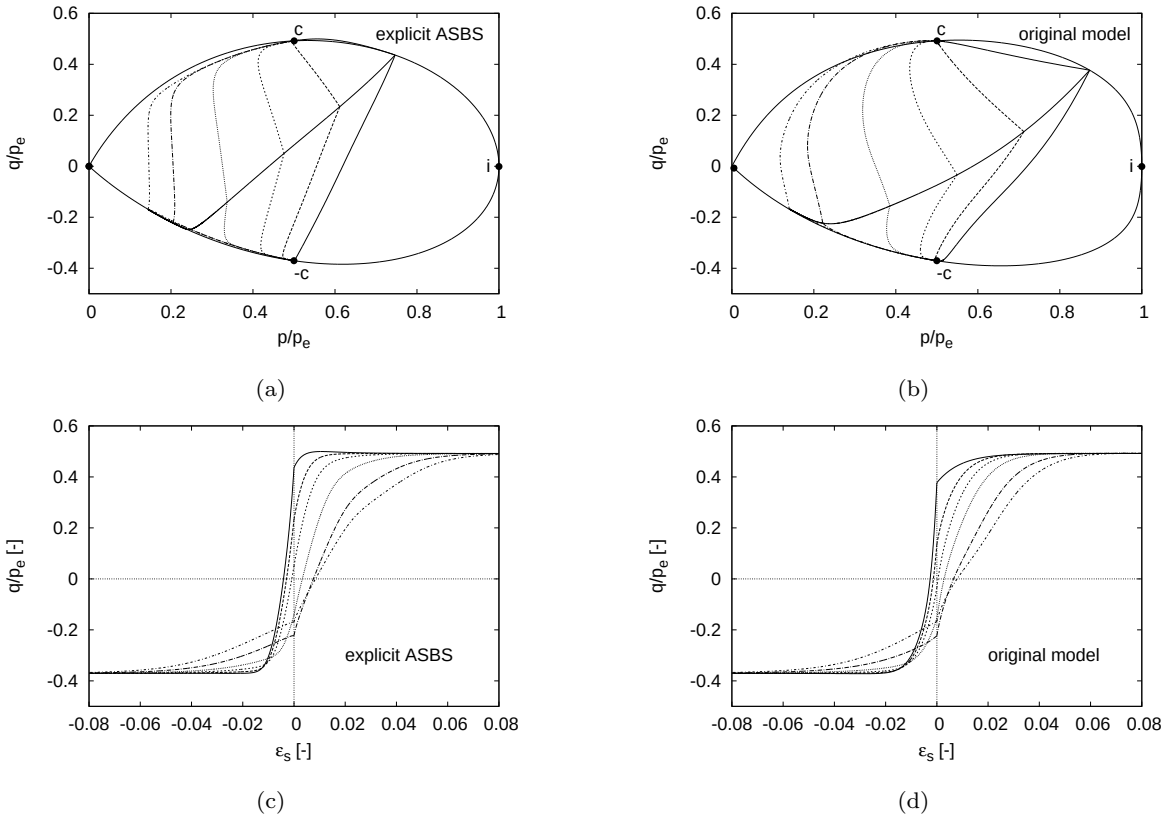

Fig. 11 Stress paths (a,b) and shear strain-deviatoric stress curves (c,d) of compression and extension undrained shear tests starting from states along K_0 unloading line.

tion pressure p_0 1000 kPa and then isotropically unloaded to the pressure $p = p_0/OCR$, from which the shear tests at constant mean stress p followed. Altogether 12 shear experiments were reported, at OCR = 1, 2.25, 2.5, 2.7, 3, 4, 5, 8, 10, 20 and 50.

Figure 12a shows stress paths in a normalised plane q/p_e vs. p/p_e, Figure 12b presents shear strain vs. deviatoric stress curves and Figure 12c shows the volumetric response. The proposed model predicts more straight approach to asymptotic states (Fig. 12a) and slightly different non-linear response inside the ASBS (lower dilatancy rate and higher peak friction angle of the overconsolidated soil). Otherwise, simulations by the two models are quite similar and they represent relatively well the experimental data.

Dortmund clay: The second investigated set of experimental data is on the overconsolidated illitic clay from tertiary deposits overlying coal seams near Dortmund, Germany. The experimental data and predictions by the original model have been presented by Herle et al. [17]. Figures 13(a,b) show stress paths of three undrained triaxial tests and predictions by the original and proposed constitutive models. The predicted stress paths differ in the way the asymptotic state is approached, but both predictions represent the experimental data reasonably well. More significant difference is clear from the predicted shear strain vs. deviatoric stress curves (Figures 13c,d). The proposed model predicts accurately the decrease of the tangent shear modulus with shear strain. On the other hand, the original model represents the stress-strain curve relatively poorly, as it underestimates the original stiffness and also the rate of the stiffness degradation.

Weald clay: Experimental data on reconstituted Weald clay by Henkel [15] and Parry [45] represent classical set of experiments used in the literature to evaluate different constitutive models. For example, these experiments have previously been adopted by Gudehus [9] in the evaluation of his visco-hypoplastic model and by Weifner and Kolymbas [50], who compared performance of different hypoplastic models for clays. Weald clay is an estuarine deposit of the Cretaceous period, in the natural state heavily overconsolidated, with index properties $w_L = 43\%$, $w_P = 18\%$ and 40% fraction of clay minerals [15]. In this evaluation, isotropic loading and unloading tests on reconstituted clay by Henkel [15] have been adopted, together with undrained triaxial compression and extension tests on normally con-

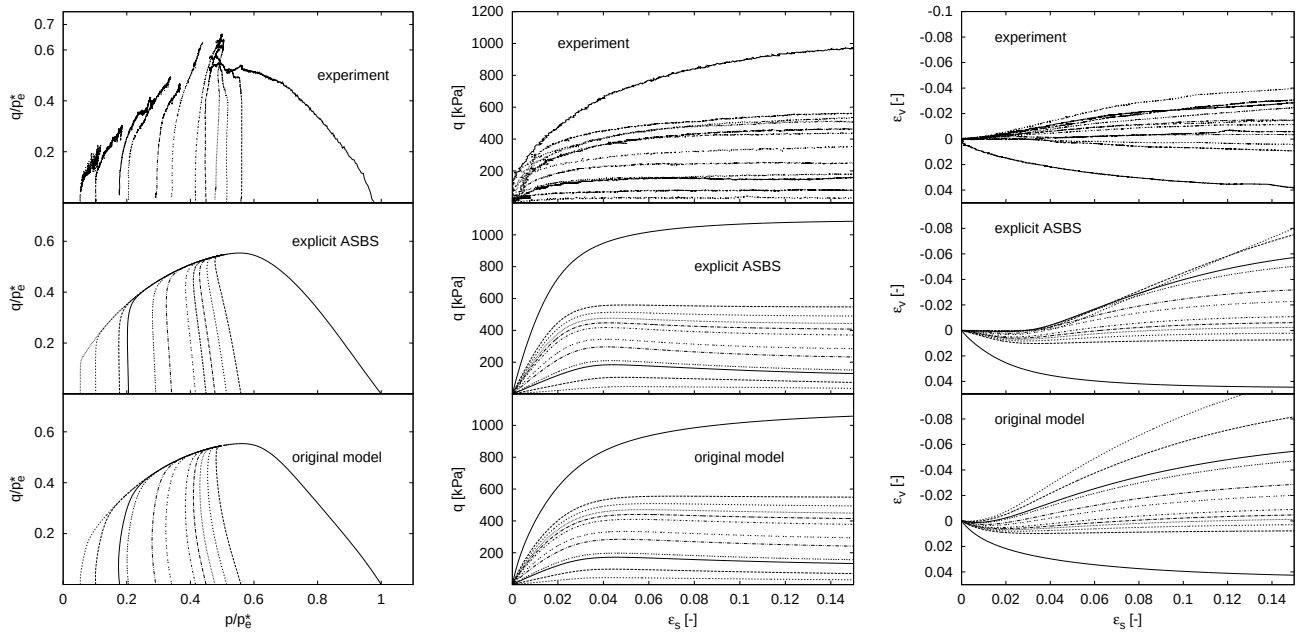

Fig. 12 Experimental results on reconstituted kaolin clay by Hattab and Hicher [14] and predictions by the proposed and original models.

solidated and overconsolidated samples published by Parry [45]. Parry [45] did not present isotropic tests, but noted that the isotropic response he observed is practically identical to that published by Henkel [15].

The parameters N, λ^* and κ^* have been calibrated using isotropic loading and unloading tests, as shown in Fig. 14. Both the models represent almost exactly both the loading and unloading curves. Note that different values of κ^* (Tab. 1) have been adopted for the two models. This is because the predictions of the isotropic unloading test differ slightly in the two models due to different formulation of the pyknotropy factor f_d. In the proposed model, the exponent α in (34) has a fixed value of 2, whereas in the original model it is a function of material parameters λ^*, κ^* and φ_c.

Simulations of the drained and undrained compression and extension tests on normally consolidated and overconsolidated samples are shown in Fig. 15; the initial states are indicated in Fig. 14. The two models yield similar predictions. The proposed model overpredicts peak strength in drained compression test on overconsolidated soil; this can be reduced by modifying the value of a from Eq. (25). The calibration yields relatively high values of the parameter κ^*. This causes the ASBS of the original model to have unrealistic shape, as shown in Fig. 16b together with normalised stress paths of the shear tests. The original model has the ASBS independent of the model parameters (Fig. 16a), and thus does not have this shortcoming. An unsatisfactory performance presented by Weifner and Kolymbas [50] has not been reproduced.

Brno clay: Brno clay is a calcareous illitic silty clay from Brno, Czech Republic. In its natural state it is of stiff to very stiff consistency and high plasticity, and forms more than 100m thick strata in Miocene marine sedimentary basin of the Carpathian fore-trough. Brno clay was studied experimentally by Svoboda et al. [48]. The original model was in Ref. [48] used in simulations of tunnels excavated by means of the New Austrian Tunnelling Method. The experimental data, together with simulation by the original and proposed models, are shown in Fig. 17. Figure 17a shows results of oedometric test on undisturbed Brno clay sample, and Figures 17b,c show stress paths and deviatoric stress - shear strain curves of undrained shear tests on undisturbed samples.

The two models yield practically identical predictions of the oedometric test. In shear, the response by the two models differ, and the difference is qualitatively the same as that observed in Dortmund clay simulations (Fig. 13). The stress paths are slightly different and, in particular, the proposed model predicts more gradual decrease of the shear stiffness with shear strain, which better agrees with the experimental data.

Koper soft silty clay: The last soil investigated is a soft silty clay from Quaternary deposits in Koper, Slovenia. The material may be characterized as a gray, high

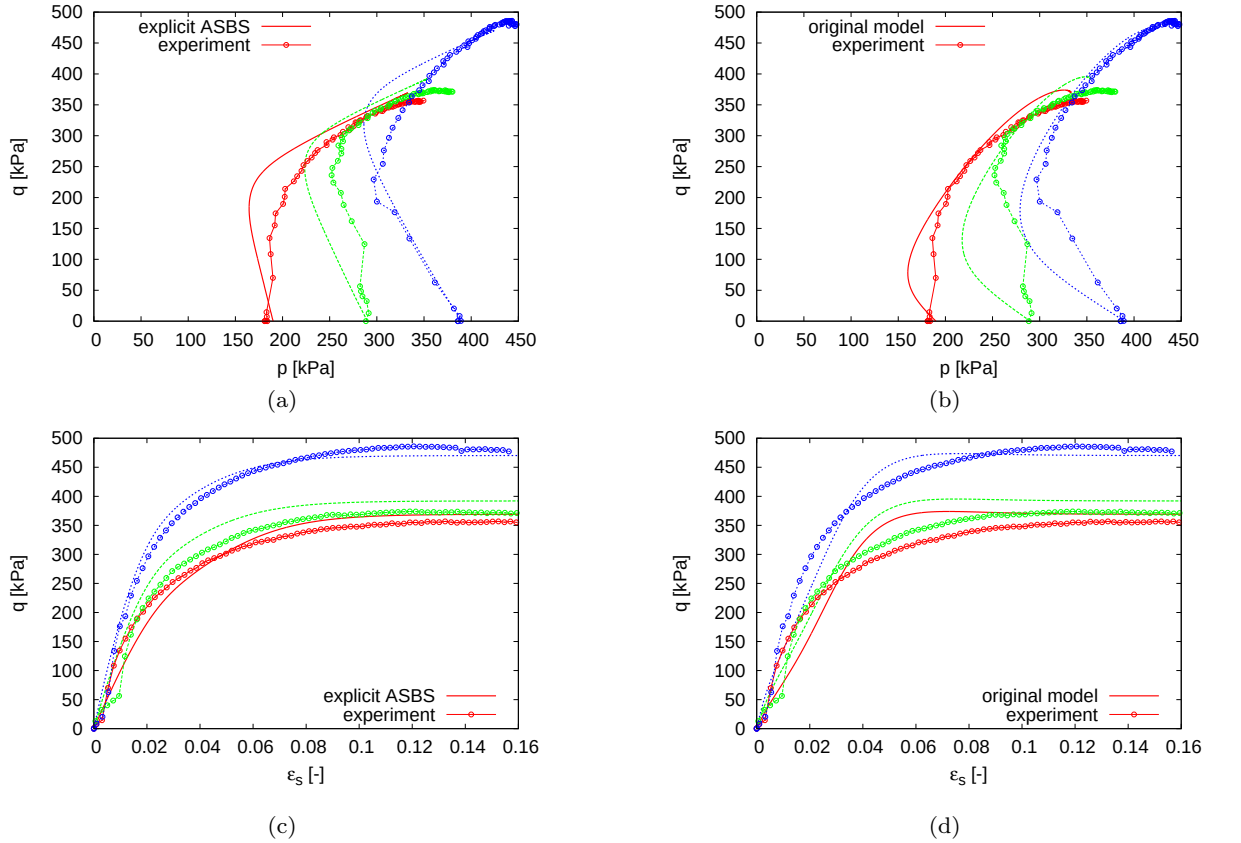

Fig. 13 Undrained triaxial tests on overconsolidated Dortmund clay and their representation by the proposed and original models. Experimental data from [17].

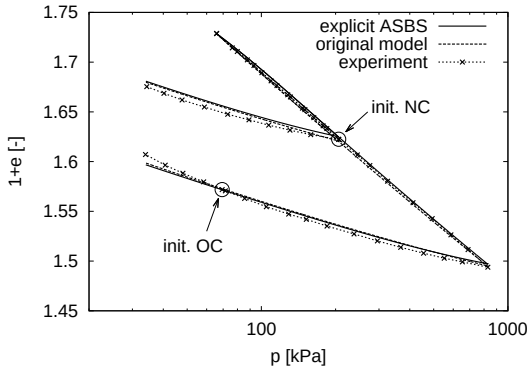

Fig. 14 Results of isotropic loading and unloading tests on reconstituted Weald clay; experimental data by Henkel [15], compared with predictions by the proposed and original models. Initial states of the shear tests on normally consolidated (NC) and overconsolidated (OC) indicated.

plasticity carbonatic silty clay with the Atterberg limits $w_L = 64\%$ and $w_P = 34\%$. Laboratory experiments, described by Mašín et al. [31], have been performed on undisturbed specimens trimmed from block samples excavated from a depth of 3.4 m. The calibrated parameters were in Ref. [31] used in simulations of a deep excavation. Figure 18 shows results of three undrained triaxial shear tests. The stress paths indicate the soil is very soft, close to normally consolidated conditions. Unlike in the case of overconsolidated clays (Figs. 13 and 17), the two models now yield very similar response.

9 Conclusions

A new hypoplastic model for fine-grained soils has been proposed. The model is based on an approach which enables us to specify explicitly the asymptotic state boundary surface and corresponding asymptotic strain rate direction. The model eliminates several shortcomings of the original clay hypoplastic model from [24] and improves its predictions, while using equivalent material parameters. The main advantage of the new model is in the independent formulation of the individual model components. The new model is thus more suitable to form a basis for further developments and enhancements.

Acknowledgements Financial support by the research grants GACR P105/12/1705, GACR P105/11/1884, TACR TA01031840 and MSM 0021620855 is greatly appreciated.

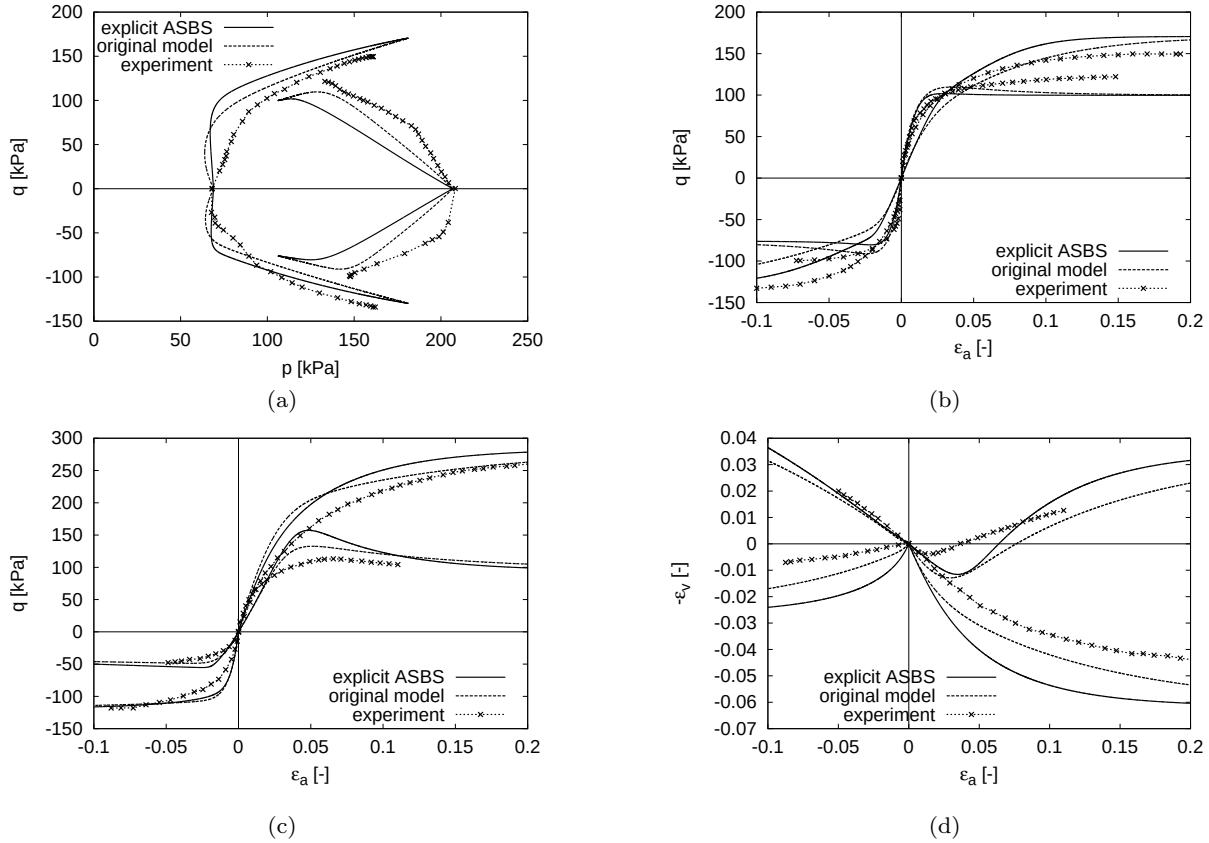

Fig. 15 Drained and undrained compression and extension tests on normally consolidated and overconsolidated samples of reconstituted Weald clay. Experimental data by Parry [45] compared with predictions by the proposed and original models.

Appendix

The Appendix summarises complete formulation of the proposed hypoplastic model. The general rate formulation reads

$$\mathring{\mathbf{T}} = f_s \boldsymbol{\mathcal{L}} : \mathbf{D} - \frac{f_d}{f_d^A} \boldsymbol{\mathcal{A}} : \boldsymbol{d} \|\mathbf{D}\| \tag{43}$$

with

$$\boldsymbol{\mathcal{L}} = \boldsymbol{\mathcal{I}} + \frac{\nu}{1-2\nu} \mathbf{1} \otimes \mathbf{1} \tag{44}$$

$$\boldsymbol{\mathcal{A}} = f_s \boldsymbol{\mathcal{L}} + \frac{\mathbf{T}}{\lambda^*} \otimes \mathbf{1} \tag{45}$$

$$f_s = \frac{3p}{2} \left(\frac{1}{\lambda^*} + \frac{1}{\kappa^*} \right) \frac{1-2\nu}{1+\nu} \tag{46}$$

where ν, λ^* and κ^* are model parameters, $p = -\operatorname{tr}\mathbf{T}/3$, and $\mathbf{1}$ and $\boldsymbol{\mathcal{I}}$ are second- and fourth order unity tensors respectively. The factor f_d reads

$$f_d = \left(\frac{2p}{p_e} \right)^{\alpha} \tag{47}$$

with $\alpha = 2$ and the equivalent pressure

$$p_e = p_r \exp \left[\frac{N - \ln(1+e)}{\lambda^*} \right] \tag{48}$$

where N is a parameter and p_r is a reference stress equal to 1 kPa. The factor f_d^A reads

$$f_d^A = 2^{\alpha} (1 - F_m)^{\alpha/\omega} \tag{49}$$

where F_m is the Matsuoka-Nakai factor calculated from

$$F_m = \frac{9 I_3 + I_1 I_2}{I_3 + I_1 I_2} \tag{50}$$

and the exponent ω reads

$$\omega = -\frac{\ln\left(\cos^2 \varphi_c\right)}{\ln 2} + a \left(F_m - \sin^2 \varphi_c \right) \tag{51}$$

where φ_c is a parameter and $a = 0.3$. The stress invariants I_1, I_2 and I_3 are given by

$$I_1 = \operatorname{tr}\mathbf{T} \tag{52}$$

$$I_2 = \frac{1}{2} \left[\mathbf{T} : \mathbf{T} - (I_1)^2 \right] \tag{53}$$

$$I_3 = \det \mathbf{T} \tag{54}$$

Finally, the asymptotic strain rate direction $\boldsymbol{d}$ is calculated as

$$\boldsymbol{d} = \frac{\boldsymbol{d}^A}{\|\boldsymbol{d}^A\|} \tag{55}$$

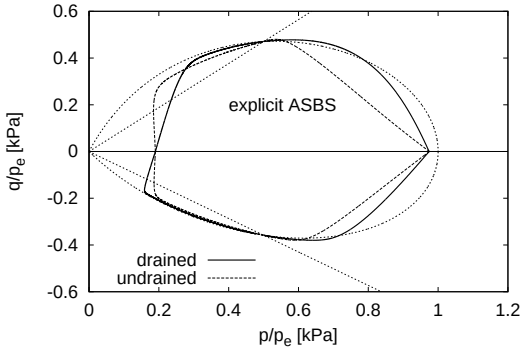

(a)

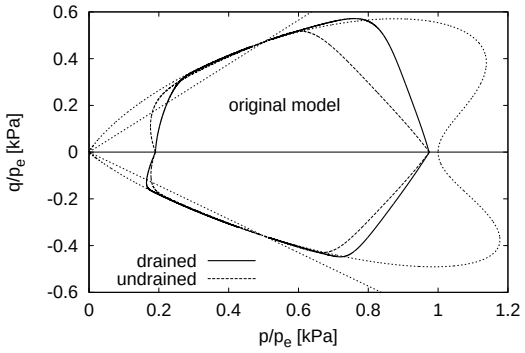

(b)

Fig. 16 The shape of the ASBS of the original and proposed model for Weald clay parameters (Tab. 1), plotted together with normalised stress paths of the shear tests from Fig. 15.

where

$$\boldsymbol{d}^A = -\hat{\mathbf{T}}^* + \mathbf{1}\left[\frac{2}{3} - \frac{\cos 3\theta + 1}{4} F_m^{1/4}\right] \frac{F_m^{\xi/2} - \sin^{\xi}\varphi_c}{1 - \sin^{\xi}\varphi_c} \tag{56}$$

with the Lode angle θ

$$\cos 3\theta = -\sqrt{6}\frac{\mathrm{tr}\left(\hat{\mathbf{T}}^* \cdot \hat{\mathbf{T}}^* \cdot \hat{\mathbf{T}}^*\right)}{\left[\hat{\mathbf{T}}^* : \hat{\mathbf{T}}^*\right]^{3/2}} \tag{57}$$

exponent ξ

$$\xi = 1.7 + 3.9\sin^2\varphi_c \tag{58}$$

and the stress measure $\hat{\mathbf{T}}^* = \mathbf{T}/\,\mathrm{tr}\,\mathbf{T} - \mathbf{1}/3$. The model requires five parameters φ_c, λ^*, κ^*, N and ν, and state variables $\mathbf{T}$ and void ratio e.

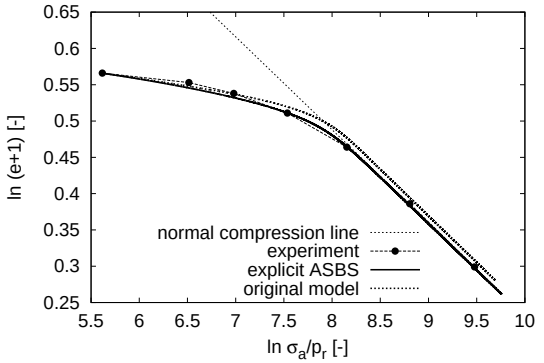

(a)

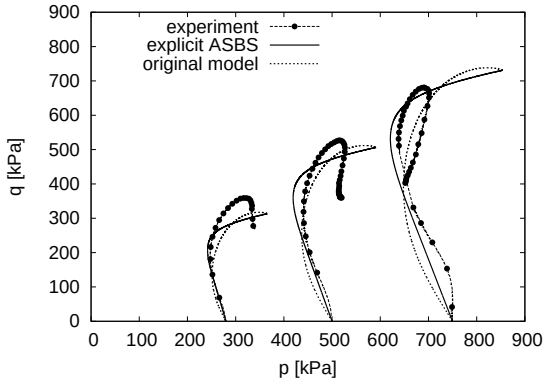

(b)

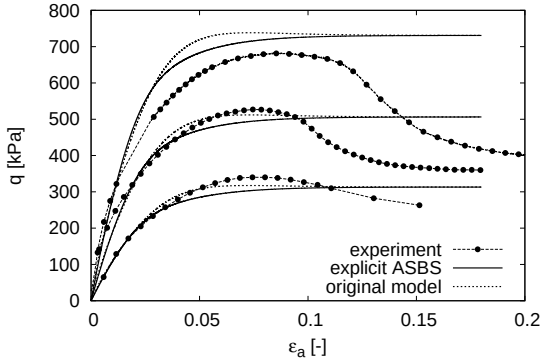

(c)

Fig. 17 Oedometric tests on undisturbed Brno clay (a), undrained triaxial shear tests on undisturbed Brno clay (b,c). Predictions by the proposed and original models; experimental data from [48].

References

1. Ali, A., Meier, T., Herle, I.: Numerical investigation of undrained cavity expansion in fine-grained soils. Acta Geotechnica **6**, 31–40 (2011)
2. Bardet, J.P.: Lode dependences for isotropic pressure-sensitive elastoplastic materials. Journal of Applied Mechanics **57**, 498–506 (1990)
3. Butterfield, R.: A natural compression law for soils. Géotechnique **29**(4), 469–480 (1979)
4. Callisto, L., Calabresi, G.: Mechanical behaviour of a natural soft clay. Géotechnique **48**(4), 495–513 (1998)
5. Chambon, R., Desrues, J., Hammad, W., Charlier, R.: CLoE, a new rate–type constitutive model for geomaterials. theoretical basis and implementation. International Journal for Numerical and Analytical Methods in Geomechanics **18**, 253–278 (1994)

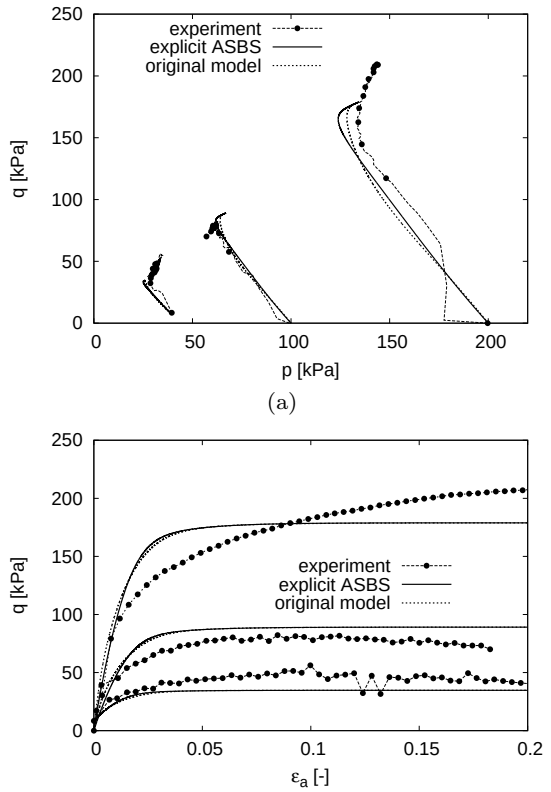

Fig. 18 Results of undrained triaxial shear tests on undisturbed Koper soft silty clay. Experimental data from [31] together with the simulations by the proposed and original models.

6. D'Onza, F., Gallipoli, D., Wheeler, S., Casini, F., Vaunat, J., Khalili, N., Laloui, L., Mancuso, C., Mašín, D., Nuth, M., Pereira, M., Vassallo, R.: Benchmark of constitutive models for unsaturated soils. Géotechnique **61**(4), 283–302 (2011)
7. Fuentes, W., Triantafyllidis, T., Lizcano, A.: Hypoplastic model for sands with loading surface. Acta Geotechnica **7**, 177–192 (2012)
8. Gudehus, G.: A comprehensive constitutive equation for granular materials. Soils and Foundations **36**(1), 1–12 (1996)
9. Gudehus, G.: A visco-hypoplastic constitutive relation for soft soils. Soils and Foundations **44**(4), 11–25 (2004)
10. Gudehus, G.: Physical Soil Mechanics. Springer, Berlin (2011)
11. Gudehus, G., Amorosi, A., Gens, A., Herle, I., Kolymbas, D., Mašín, D., Muir Wood, D., Nova, R., Niemunis, A., Pastor, M., Tamagnini, C., Viggiani, G.: The soilmodels.info project. International Journal for Numerical and Analytical Methods in Geomechanics **32**(12), 1571–1572 (2008)
12. Gudehus, G., Mašín, D.: Graphical representation of constitutive equations. Géotechnique **59**(2), 147–151 (2009)
13. Hájek, V., Mašín, D., Boháč, J.: Capability of constitutive models to simulate soils with different OCR using a single set of parameters. Computers and Geotechnics **36**(4), 655–664 (2009)
14. Hattab, M., Hicher, P.Y.: Dilating behaviour of overconsolidated clay. Soils and Foundations **44**(4), 27–40 (2004)
15. Henkel, D.J.: The effect of overconsolidation on the behaviour of clays during shear. Géotechnique **6**, 139–150 (1956)
16. Herle, I., Kolymbas, D.: Hypoplasticity for soils with low friction angles. Computers and Geotechnics **31**(5), 365–373 (2004)
17. Herle, I., Mašín, D., Kostkanová, V., Karcher, C., Dahmen, D.: Experimental investigation and theoretical modelling of soft soils from mining deposits. In: C.K. Chung, Y.H. Jung, H.K. Kim, J.S. Lee, D.S. Kim (eds.) Proc. 5^{th} International Symposium on Deformation Characteristics of Geomaterials, Seoul, Korea, vol. 2, pp. 858–864 (2011)
18. Huang, W.X., Wu, W., Sun, D.A., Sloan, S.: A simple hypoplastic model for normally consolidated clay. Acta Geotechnica **1**(1), 15–27 (2006)
19. Jáky, J.: Pressures in silos. In: Proc. 2^{nd} Int. Conf. Soil Mechanics, vol. 1, pp. 103–107. Rotterdam (1948)
20. Kirkgard, M.M., Lade, P.V.: Anisotropic three–dimmensional behaviour of a normally consolidated clay. Canadian Geotechnical Journal **30**, 848–858 (1993)
21. Kolymbas, D.: Computer-aided design of constitutive laws. International Journal for Numerical and Analytical Methods in Geomechanics **15**, 593–604 (1991)
22. Kolymbas, D., Herle, I.: Shear and objective stress rates in hypoplasticity. International Journal for Numerical and Analytical Methods in Geomechanics **27**, 733–744 (2003)
23. Matsuoka, H., Nakai, T.: Stress–deformation and strength characteristics of soil under three different principal stresses. In: Proc. Japanese Soc. of Civil Engineers, vol. 232, pp. 59–70 (1974)
24. Mašín, D.: A hypoplastic constitutive model for clays. International Journal for Numerical and Analytical Methods in Geomechanics **29**(4), 311–336 (2005)
25. Mašín, D.: A hypoplastic constitutive model for clays with meta-stable structure. Canadian Geotechnical Journal **44**(3), 363–375 (2007)
26. Mašín, D.: 3D modelling of a NATM tunnel in high K_0 clay using two different constitutive models. Journal of Geotechnical and Geoenvironmental Engineering ASCE **135**(9), 1326–1335 (2009)
27. Mašín, D.: Comparison of predictive capabilities of selected elasto-plastic and hypoplastic models for structured clays. Soils and Foundations **49**(3), 381–390 (2009)
28. Mašín, D.: Predicting the dependency of a degree of saturation on void ratio and suction using effective stress principle for unsaturated soils. International Journal for Numerical and Analytical Methods in Geomechanics **34**, 73–90 (2010)
29. Mašín, D.: Asymptotic behaviour of granular materials. Granular Matter (in print, DOI: 10.1007/s10035-012-0372-x) (2012)
30. Mašín, D.: Hypoplastic Cam-clay model. Géotechnique **62**(6), 549–553 (2012)
31. Mašín, D., Boháč, J., Tůma, P.: Modelling of a deep excavation in a silty clay. In: Proc. 15^{th} European Conference on Soil Mechanics and Geotechnical Engineering, vol. 3, pp. 1509–1514 (2011)
32. Mašín, D., Herle, I.: State boundary surface of a hypoplastic model for clays. Computers and Geotechnics **32**(6), 400–410 (2005)
33. Mašín, D., Herle, I.: Improvement of a hypoplastic model to predict clay behaviour under undrained conditions. Acta Geotechnica **2**(4), 261–268 (2007)
34. Mašín, D., Khalili, N.: A hypoplastic model for mechanical response of unsaturated soils. International Journal

for Numerical and Analytical Methods in Geomechanics **32**(15), 1903–1926 (2008)
35. Mašín, D., Khalili, N.: A thermo-mechanical model for variably saturated soils based on hypoplasticity. International Journal for Numerical and Analytical Methods in Geomechanics (in print, DOI: 10.1002/nag.1058) (2011)
36. Mašín, D., Tamagnini, C., Viggiani, G., Costanzo, D.: Directional response of a reconstituted fine grained soil. Part II: performance of different constitutive models. International Journal for Numerical and Analytical Methods in Geomechanics **30**(13), 1303–1336 (2006)
37. Miča, L., Chalmovský, J., Fiala, R., Račandský, V.: Numerical analysis of retaining structures of excavations (in Czech). Akademické nakladatelství CERM, Brno, Czech Republic, ISBN 978-80-7204-773-4, 142 pages (2012)
38. Najser, J., Mašín, D., Boháč, J.: Numerical modelling of lumpy clay landfill. International Journal for Numerical and Analytical Methods in Geomechanics **36**(1), 17–35 (2012)
39. Niemunis, A.: Extended Hypoplastic Models for Soils. Habilitation thesis, Ruhr-University, Bochum (2003)
40. Niemunis, A., Grandas Tavera, C.E., Prada Sarmiento, L.F.: Anisotropic visco-hypoplasticity. Acta Geotechnica **4**(4), 293–314 (2009)
41. Niemunis, A., Herle, I.: Hypoplastic model for cohesionless soils with elastic strain range. Mechanics of Cohesive-Frictional Materials **2**, 279–299 (1997)
42. Niemunis, A., Prada Sarmiento, L.F., Grandas Tavera, C.E.: Extended paraelasticity and its application to a boundary value problem. Acta Geotechnica **6**, 91–92 (2011)
43. Niemunis, A., Prada Sarmiento, L.F., Grandas Tavera, C.E.: Paraelasticity. Acta Geotechnica **6**, 67–80 (2011)
44. Niemunis, A., Wichtmann, T., Triantafyllidis, T.: A high-cycle accumulation model for sand. Computers and Geotechnics **32**, 245–263 (2005)
45. Parry, R.H.G.: Triaxial compression and extension tests on remoulded saturated clay. Géotechnique **10**, 166–180 (1960)
46. Roscoe, K.H., Burland, J.B.: On the generalised stress-strain behaviour of wet clay. In: J. Heyman, F.A. Leckie (eds.) Engineering Plasticity, pp. 535–609. Cambridge University Press, Cambridge (1968)
47. Svoboda, T., Mašín, D.: Comparison of displacement fields predicted by 2D and 3D finite element modelling of shallow NATM tunnels in clays. Geotechnik **34**(2), 115–126 (2011)
48. Svoboda, T., Mašín, D., Boháč, J.: Class A predictions of a NATM tunnel in stiff clay. Computers and Geotechnics **37**(6), 817–825 (2010)
49. Weifner, T., Kolymbas, D.: A hypoplastic model for clay and sand. Acta Geotechnica **2**(2), 103–112 (2007)
50. Weifner, T., Kolymbas, D.: Review of two hypoplastic equations for clay considering axisymmetric element deformations. Computers and Geotechnics **35**, 760–774 (2008)
51. von Wolffersdorff, P.A.: A hypoplastic relation for granular materials with a predefined limit state surface. Mechanics of Cohesive-Frictional Materials **1**, 251–271 (1996)
52. Wood, D.M.: Some aspects of the mechanical behaviour of kaolin under truly triaxial conditions of stress and strain. Ph.D. thesis, University of Cambridge (1974)
53. Wu, W., Bauer, E.: A simple hypoplastic constitutive model for sand. International Journal for Numerical and Analytical Methods in Geomechanics **18**, 833–862 (1994)
54. Youwai, S., Chattanjai, P., Jongpradist, P., Kongkitkul, W.: Hypoplastic model for simulation of deformation characteristics of bangkok soft clay with different stress paths. ASCE Geotechnical Special Publication **200 GSP**, 160–165 (2010)